buildings

MDPI

Article

Bending Test of Rectangular High-Strength Steel Fiber-Reinforced Concrete-Filled Steel Tubular Beams with Stiffeners

Shiming Liu [1,2,*], Zhaoyang Ji [1], Shangyu Li [1], Xiaoke Li [2], Yongjian Liu [3,*] and Shunbo Zhao [2,4,*]

1 School of Civil Engineering and Communication, North China University of Water Resources and Electric Power, Zhengzhou 450045, China
2 International Joint Research Lab for Eco-Building Materials and Engineering of Henan, North China University of Water Resources and Electric Power, Zhengzhou 450045, China
3 School of Highway, Chang'an University, Xi'an 710064, China
4 Collaborative Innovation Center for Efficient Utilization of Water Resources, North China University of Water Resources and Electric Power, Zhengzhou 450046, China
* Correspondence: liushm@ncwu.edu.cn (S.L.); lyj.chd@gmail.com (Y.L.); sbzhao@ncwu.edu.cn (S.Z.)

Abstract: To better understand the bending performance of rectangular high-strength steel fiber-reinforced concrete (HSFRC)-filled steel tubular (HSFRCFST) beams with internal stiffeners, ten beams were subjected to a four-point bending test. The primary considerations were the strength grade of the HSFRC, the steel fiber content, the internal stiffener type, and the circular hole spacing of the perfobond stiffener. The moment–curvature and flexural load–deflection curves were calculated. The mode of failure and the distribution of cracks of the infill HSFRC were observed. The presence of steel fibers greatly improved the bending stiffness and moment capacity of HSFRCFST beams, with the optimal effect happening at a steel fiber content of 1.2% by volume, according to the experimental findings. The type of stiffener influenced the failure modes of the exterior rectangular steel tube, which were unaffected by the compressive strength of the infill HSFRC. On the tension surface of HSFRCFST beams, the crack spacing of the infill HSFRC was virtually identical to the circular hole spacing of perfobond stiffeners. When the circular hole spacing was between two and three times the diameter, the perfobond stiffener worked best with the infill HSFRC. The test beams' ductility index was greater than 1.16, indicating good ductility. The test beams' rotational capacities ranged from 6.26 to 13.20, which were greater than 3.0 and met the requirements of the specification. The experimental results demonstrate that a reasonable design of the steel fiber content and the spacing between circular holes of perfobond stiffeners can significantly improve the bending resistance of rectangular HSFRCFST beams. This provides relevant parameter design suggestions for improving the ductility and bearing capacity of steel fiber-reinforced concrete beams in practical construction. Finally, a design formula for the moment capacity of rectangular HSFRCFST beams with stiffeners is presented, which corresponds well with the experimental findings.

Keywords: concrete-filled steel tubular beams; rectangular section; high-strength steel fiber-reinforced concrete; perfobond stiffener; flexural capacity

Citation: Liu, S.; Ji, Z.; Li, S.; Li, X.; Liu, Y.; Zhao, S. Bending Test of Rectangular High-Strength Steel Fiber-Reinforced Concrete-Filled Steel Tubular Beams with Stiffeners. *Buildings* **2024**, *14*, 3678. https://doi.org/10.3390/buildings14113678

Academic Editor: Mohamed K. Ismail

Received: 23 October 2024
Revised: 15 November 2024
Accepted: 18 November 2024
Published: 19 November 2024

1. Introduction

Beams, columns, towers, arch ribs, and piers made of concrete-filled steel tube (CFST) structural components are becoming more prevalent in tall buildings [1–3] and large-span bridges [4,5] due to the strong compressive resistance of infill concrete and the adaptability of exterior steel tubes. In general, the bearing capacity of infill concrete increases when it is confined by an exterior steel tube subjected to triaxial compression, and the support provided by the infill concrete prevents the external steel tube from local buckling sooner [6,7]. In addition to enhancing the deformability and bearing capacity

of CFST structural components, the combined effects of external steel tubes and infill concrete provide excellent seismic resistance and damping performance. In addition, CFST components use exterior steel tubes as the formwork to reduce the labor force required for reinforced concrete structures, shorten the construction period, and reduce engineering expenses [8–12].

In contrast to CFST columns subjected to compression or compression with flexure, CFST beams subjected to flexure have weaker infill concrete confinement by external steel tubes [13–18]. This permits the investigation required to determine the bending behavior of CFST beams [19,20]. Compared to a circular section [21,22] and an elliptical section [23,24], a rectangular or square section for CFST beams has advantages in connecting and cooperating with other members. In rectangular CFST beams, unequal bending capacity along different axes is a characteristic of their mechanical behavior. In the meantime, the lateral confinement of infill concrete by steel tubes becomes less uniform and weaker, leading to a decrease in flexural capacity and ductility [25,26].

CFST beams with a rectangular section have been enhanced using a variety of techniques. One method involved the interfacial bonding of infill concrete to steel tubes. When using high-strength concrete as infill concrete, it is important to avoid significant volume shrinkage [27–30]. Internal stiffeners efficiently increase the bonding behavior and stiffness of external steel tubes, delaying the onset of local buckling [31–35]. This encourages the investigation of internal stiffeners, such as steel plate stiffeners and perfobond stiffeners with circular holes spaced equally apart. The deficiency results in an unavoidable increase in construction costs. Alternately, one might boost the exterior steel tube and infill concrete's already impressive performance. Thick steel plates can improve the load carrying capability and ductility of CFST beams, notwithstanding the unavoidable increase in welding difficulty and construction expense [36–42]. Concrete with high strength can improve bearing capacity and energy absorption while decreasing ductility. Rubberized concrete is an eco-friendly building material that can increase ductility while decreasing structure members' compressive performance [43,44]. SFRC is advantageous for enhancing the ductility and load-bearing capacity of CFST beams [45,46]. Due to steel fibers' bridge effect on the cracks in the concrete matrix, SFRC exhibits superior post-crack behavior, impact resistance, tensile strength, and interfacial bonding strength to steel tubes [47–49]. The main parameters include the strength grade of infill concrete, which ranges from 30 MPa to 70 MPa; the percentage of steel fiber volume, ranging from 0.5% to 1.5%; and the steel fiber type, comprising straight, hooked-end, and crimped fibers. Steel fibers improve CFST beams' bearing capacity, ductility, and energy dissipation, while steel fibers with hooked ends outperform straight or crimped steel fibers [50,51]. Along with self-compacting and high-flowing construction, the orientation of steel fibers in an SFRC mixture agrees with the flexural state of the beam, and HSFRC becomes able to be used in CFST beams [52,53].

Based on the preceding statement [54], it is worthwhile to investigate the flexural behavior of rectangular high-strength steel fiber-reinforced concrete (HSFRC)-filled steel tubular (HSFRCFST) beams. In this article, the four-point bending experiment was conducted on nine HSFRCFST beams and one CFST beam used as a reference. The strength grade of HSFRC, steel fiber content, the internal stiffener type, and the circular hole spacing of perfobond stiffeners were the research factors. On the basis of test results, the failure modes, moment–curvature curves, flexural load–deflection curves, ductility indexes, rotational capacities, bending stiffnesses, and ultimate loads of test beams are discussed. Finally, suggested formulas for calculating the bending capacity of rectangular HSFRCFST are presented.

2. Materials and Methods

2.1. Concrete Preparation

One conventional concrete with an 80 MPa designed cubic compressive strength and five HSFRC mixes with 50 MPa, 60 MPa, and 80 MPa designed cubic compressive strengths were manufactured. Table 1 shows the proportions of the designed concrete. The mixes identified with "SC" and "CC" refers to HSFRC and conventional concrete,

respectively. The figures that follow show the desired cubic compressive strength as well as the proportion of steel fiber volume. The primary components of HSFRC were 42.5 R Portland cement, slag powder, water, high-quality river sand, a maximum particle size of 20 mm for graded crushed stone, hooked-end steel fiber, and a highly efficient water reducer. The fluidity of the HSFRC slump was greater than 550 mm. The length, diameter, and tensile strength of the hooked-end steel fiber were 30 mm, 0.75 mm, and 600 MPa, respectively. In the design of mixtures with different proportions of steel fiber volume, to optimize the mechanical properties and workability of the concrete, the dosage of sand and crushed stone varied. The main reason was that the fineness modulus of river sand particles was moderate, which was conducive to improving the workability of concrete, and the surface area was large, which could form better bonding with cement slurry and facilitate the dispersion and anchoring of steel fibers in concrete. So, according to the steel fiber content and the strength grade of concrete, we adjusted the ratio of river sand and gravel reasonably. In the case of high steel fiber content, the amount of river sand was increased and the amount of crushed stone was reduced.

Table 1. Mix proportions of conventional concrete and HSFRC.

Identifier	Dosage of Raw Materials (kg/m^3)						
	Cement	Slag Powder	Water	River Sand	Crushed Stone	Steel Fiber	Water Reducer
SC50/1.2	470.7	0	193	655.8	1022.4	94.2	3.3
SC60/1.2	583.3	0	175	754.4	865.9	94.2	5.9
CC80/0	535.6	133.9	170	587.3	1000.0	0	0.3
SC80/0.8	544.0	136.0	170	732.8	949.2	62.8	0.3
SC80/1.2	544.0	136.0	170	775.3	892.5	94.2	0.3
SC80/1.6	544.0	136.0	170	835.5	816.6	125.6	0.3

2.2. Fabrication of Test Beams

Ten test beams were constructed. There were perfobond stiffeners on eight of them, steel plate stiffeners on one, and none on the last one. All the test beams had a length of 1200 mm and a cross-section measuring 360 mm by 188 mm. Steel tubes and internal stiffeners were fabricated from 4 mm thick steel plates. Additional information regarding the stiffened test beams is shown in Figure 1. In every respect, the test beam without a stiffener was identical to the test beams with stiffeners.

The test beams were developed and produced in compliance with China's GB/T 50081 [55], JG/T472 [56], and GB 50666 [57] specifications, as well as GB50661 [58] and DG/TJ08 [59] for the construction of steel structures, including installation and welding. A forced trough mixer was implemented for ordinary concrete and HSFRC. Using a welding machine with an automatically changeable parameter, steel plates were welded. Using a portable ultrasound device, the weld quality was evaluated.

The production of steel fiber-reinforced concrete adopts a dry wet process, with materials added in the order of river sand, steel fibers, crushed stone, slag powder, and cement. The mixture is first dry mixed in the mixer, and then wet mixed with water and water reducer. When adding steel fibers, a steel fiber dispersing device is used, and the steel fibers are dispersed by a disperser before entering the forced mixer. Here, steel sheets were used to construct both the outer rectangular steel tubes and the internal stiffeners. The perfobond stiffener's circular holes were precisely drilled. Using sandblasting, rust was removed from the prepared steel members. Internal ribs were used to stiffen rectangular steel tubes. The specimen was then maintained in a vertical position on the thick steel plate. The infill HSFRC was cast in layers into the rectangular steel tube and immediately vibrated with an electric vibrator to remove air pockets. A coating of high-grade cement mortar was put on the infill HSFRC's upper surface to smooth it. The test beams were then covered in straw and sprayed with water at room temperature for 28 days. Three cube test pieces with 150 mm side lengths and three prism test pieces with 150 mm × 150 mm × 300 mm sizes were cast and cured alongside each test beam under the same conditions.

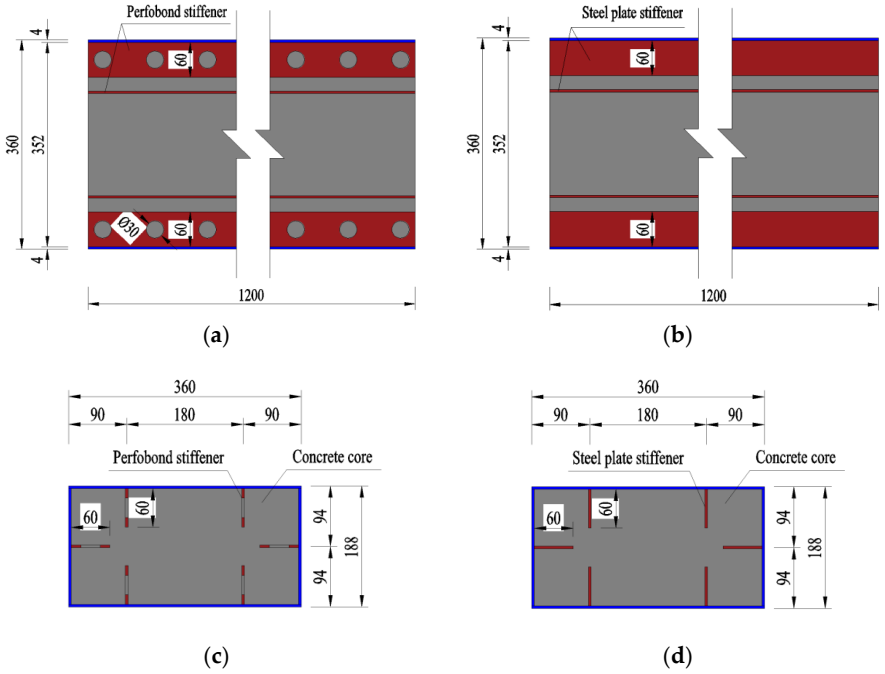

Figure 1. Specifications for beams with various stiffeners (unit: mm). (**a**) Horizontal section of perfobond stiffeners. (**b**) Horizontal section of steel plate stiffeners. (**c**) Sectional view of perfobond stiffeners. (**d**) Sectional view of steel plate stiffeners.

2.3. Material Properties

According to the criteria of China code GB/T 228.1 [60], tensile tests were conducted on the steel plates to determine their tensile qualities. Three samples were tested as a group. The average values for elasticity modulus, yield strength, and ultimate tensile strength, as obtained by testing, were 206 GPa, 360 MPa, and 576 MPa, respectively.

Using China code GB/T 50081, the cubic and prismatic compressive strengths of infill HSFRC were measured and expressed as f_{cu} and f_c, respectively. Table 2 displays the results of the experiment. In the following table, PS, SS, and NS denote test beams with perfobond stiffener, steel plate stiffener, and no stiffener, respectively. This is followed by perfobond stiffener circular hole spacing, infill concrete target strength grade, and steel fiber volume percentage (v_f). Using the Chinese standard GB 50936 [61], the test beam confinement coefficient θ was computed.

$$\theta = \frac{f_{yt} A_{st}}{f_c A_c} \tag{1}$$

Table 2. Strength of infill concrete and stiffener details of test beams.

Identifier	v_f (%)	f_{cu} (MPa)	f_c (MPa)	θ	Hole Spacing (mm)	Stiffener Type
PS-120-SC80/1.2	1.2	85.0	53.0	0.47	120	Perfobond stiffener
PS-90-SC80/1.2	1.2	67.0	42.7	0.59	90	
PS-60-SC80/1.2	1.2	65.3	41.7	0.6	60	
PS-60-SC80/0.8	0.8	81.0	50.8	0.49	60	
PS-60-SC80/1.6	1.6	78.3	49.3	0.51	60	
PS-60-SC50/1.2	1.2	46.0	30.2	0.83	60	
PS-60-SC60/1.2	1.2	54.0	34.8	0.72	60	
PS-60-CC80/0	0	80.0	50.2	0.50	60	
SS-0-SC80/1.2	1.2	88.0	54.6	0.46	--	Steel plate stiffener
NS-0-SC80/1.2	1.2	77.0	48.5	0.51	--	No stiffener

In this equation, f_{yt} represents the actual measured yield strength of the outer rectangular steel tube in MPa, while A_c and A_{st} are the cross-sectional areas of the infill concrete and the outside rectangular steel tube, both expressed in mm^2.

2.4. Test Preparation and Procedure

The test apparatus and arrangement are depicted in Figure 2. Before the tests, black grids measuring 30 mm by 50 mm were drawn on the outside of the steel tubes to see if there was any local buckling. The test beams were bent using hydraulic-servo test equipment with a capacity of 5000 kN in a four-point configuration until failure. The rolled hinge bearings supported the test beams with an effective span of 1000 mm. The proportion of shear span to effective depth was equal to 1.36. The load sensor was mounted in the middle of the rigid I-girder, which distributed the load across the I-girder. Before the load was lower than 70% of the matching predicted maximum capacity, it was being loaded at a rate of 0.5 kN/s. After that, the loading method adjusted the speed of the displacement control to be 0.5 mm/min. When the midspan displacement reached 1/200 of the effective span, the experiment was ended. To measure the vertical deflection, five linear variable differential transducers (LVDTs) with deformation limits of 50 mm were attached at the support, load sections, and midspan. In order to eliminate the effect of support displacements, the vertical deflection of test beams was computed using Formula (2).

$$\delta_{ai} = \delta_{mi} - \frac{(\delta_{m1} + \delta_{m5})}{2},\ i = 2,\ 3,\ 4, \tag{2}$$

where δ_{ai} is the vertical deflection of test beam in mm, δ_{ai} is the vertical displacement measured at sections of test beam in mm, and δ_{m1} and δ_{m5} are the displacements measured at the left and right support in mm, respectively.

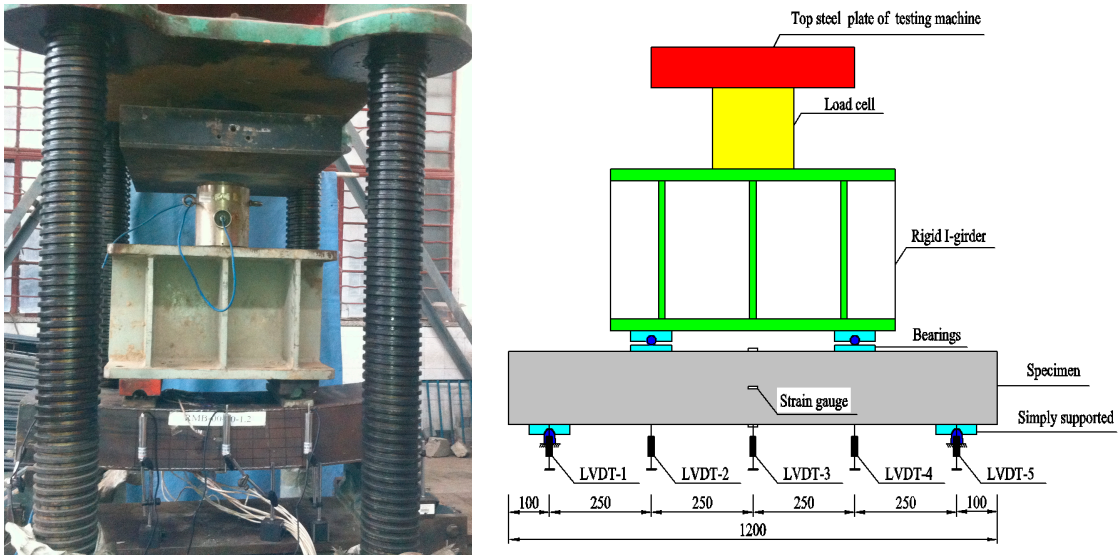

(**a**) Spots photo (**b**) Schematic diagram

Figure 2. Experiment setup and instrumentation (unit: mm).

To analyze the stress condition of the rectangular steel tube during the test, eight and twelve strain gauges were, respectively, positioned in the midspan of the test beam without stiffeners and with stiffeners. The test beam without stiffeners and with stiffeners' sketch map as shown in Figure 3. Using a steel ruler with a 200 mm range, the relative movement between the outside rectangular steel tube and the infill HSFRC was measured. The acquisition system simultaneously displayed all corresponding data.

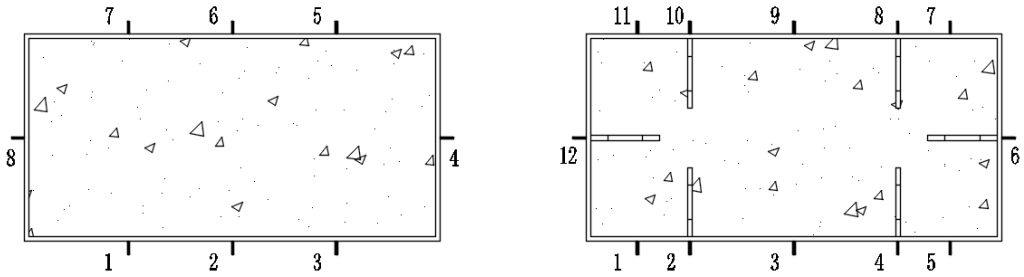

(**a**) No stiffener (**b**) With stiffeners

Figure 3. Strain gauges of the midspan section layout.

3. Test Results and Discussions

3.1. Failure Modes

The typical modes of failure for HSFRCFST beams are illustrated in Figure 4. Each of the specimens appeared to have two buckling failure modes on the upper surface and exhibited some ductility when loaded. When the specimen's applied load reached 20–30% of its maximum capacity, the specimen emitted a slight abnormal noise that gradually diminished and became intermittent. It is believed that a local bond failure occurred between the exterior steel plate and the infill HSFRC. On the compression surface of the rectangular steel tube, a few wrinkles appeared as the applied load approached its maximum. The vertical deflection was minimal due to the significant bending stiffness of HSFRCFST beams. Compared to HSFRCFST beams stiffened with a steel plate or without stiffeners, where the relative slippage between the outside rectangular steel tube and the infill HSFRC was greater than 6 mm, the relative slip of HSFRCFST beams stiffened with perfobond stiffeners was negligible (i.e., 1 mm).

As shown in Figure 4, local buckling of the outside rectangular steel tube at the midspan of the HSFRCFST beam stiffened with perfobond plates. The welded seam on the compression face of a test beam stiffened with steel plate stiffeners or without stiffeners was torn and damaged, and the buckling of the exterior rectangular steel tube was insignificant. This illustrates that the failure modes of HSFRCFST beams are significantly affected by the type of internal stiffener used. In contrast, the failure modes were not noticeably impacted by either the compression grade of infill HSFRC or the inclusion of steel fibers.

Local buckling of the upper surface was seen in the center of the stiffeners, as depicted in Figure 5 regarding the appearance of the midspan section. The stiffeners effectively restricted the growth of local buckling along the upper edge. In the absence of a stiffener, the upper edge of the HSFRCFST beam buckled outward along its entire length.

Following the loading test, the outside rectangular steel tube was cut away using an oxygen–acetylene flame in order to inspect and assess the damage to the infill HSFRC. The infill HSFRC that corresponded to the buckling of steel tubes was crushed. Figure 6 depicts the tensile side appearances of infill HSFRC on some of the test beams with perfobond stiffeners. The cracks of the internal infill HSFRC were not penetrated, and the crack spacing was roughly equivalent to the circular hole spacing of perfobond stiffeners. It is speculated that the concrete dowel in the perfobond stiffeners contributed to the stiffener's stress and was in a complex state of stress. This indicates that a concrete dowel can reliably transmit the force of an exterior rectangular steel tube through perfobond stiffeners. The presence of steel fibers in infill HSFRC had a negligible impact on crack spacing. It is essential to point out that the steel fibers at the crack were extracted whole and undamaged. This confirms that steel fibers with tensile strengths of more than 600 MPa were adequate for HSFRCFST beams subjected to pure bending.

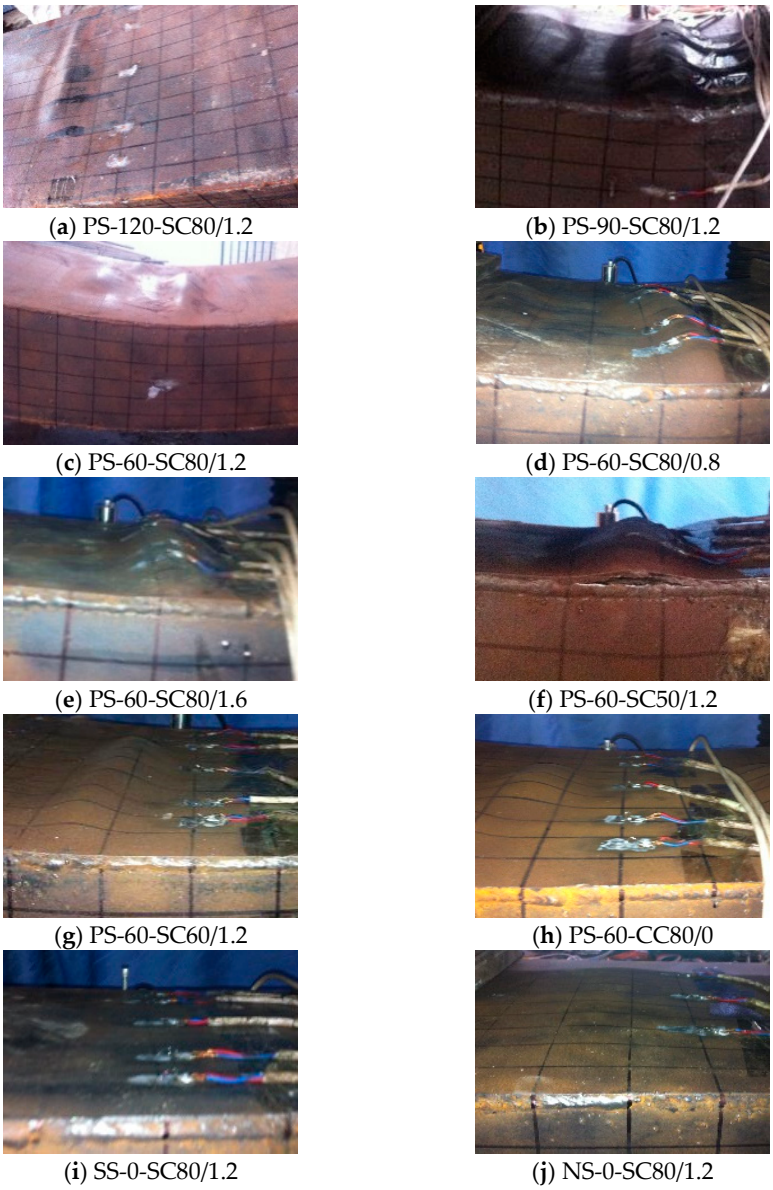

(**a**) PS-120-SC80/1.2 (**b**) PS-90-SC80/1.2

(**c**) PS-60-SC80/1.2 (**d**) PS-60-SC80/0.8

(**e**) PS-60-SC80/1.6 (**f**) PS-60-SC50/1.2

(**g**) PS-60-SC60/1.2 (**h**) PS-60-CC80/0

(**i**) SS-0-SC80/1.2 (**j**) NS-0-SC80/1.2

Figure 4. Failure modes of the beams.

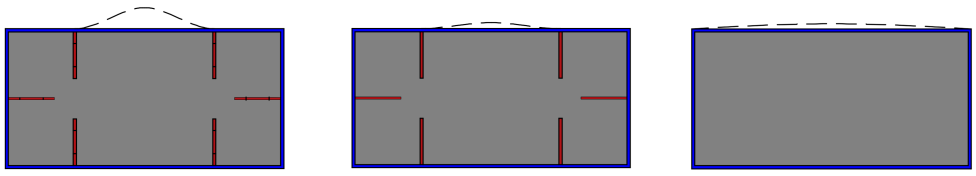

(**a**) With perfobond stiffeners (**b**) With steel plate stiffeners (**c**) No stiffener

Figure 5. The appearance of the midspan section of the HSFRCFST beams.

From the experimental results obtained after loading, it can be seen that compared with ordinary steel plate stiffeners, perforated steel plate stiffeners reduced the occurrence of local cracks and delay the development of cracks. This was due to the significant enhancement of the combination effect between steel tubes and infilled concrete by perfobond stiffeners, which improved the overall performance of rectangular HSFRCFST with stiffeners. This combination effect helped to distribute the load more evenly in the beam, thereby reducing the risk of local stress concentration and minimizing the occurrence of local cracks of infilled concrete.

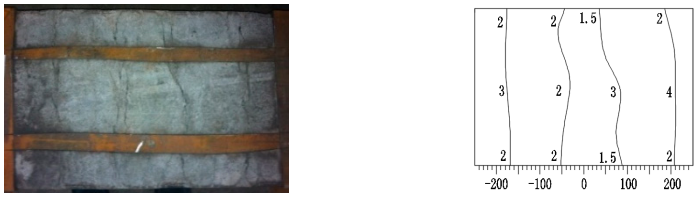

(**a**) PS-120-SC80/1.2

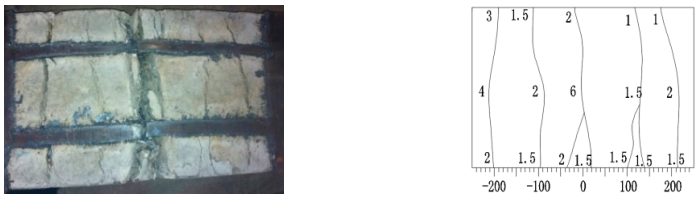

(**b**) PS-90-SC80/1.2

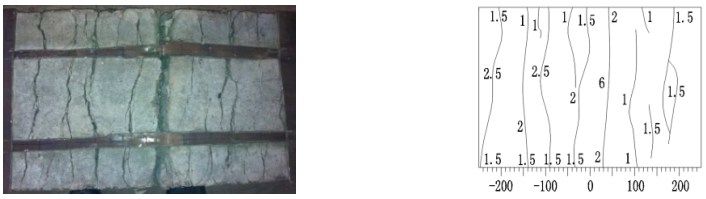

(**c**) PS-60-SC80/1.2

(**d**) PS-60-CC80/0

(**e**) PS-60-SC80/0.8

(**f**) PS-60-SC80/1.6

Figure 6. Failure modes and crack distribution of the infill concrete (unit: mm).

3.2. Vertical Deflection Curves

Figure 7 depicts the experimentally determined curves of vertical deflection along the length. While the development of vertical displacement at various points along the span is essentially synchronous for initial loads, for higher load levels, the vertical deflection at midspan develops dramatically, while that at other points grows uniformly. At every load level, the predicted values of the half-sine curve closely match the experimental values. The vertical displacement curve can therefore be expressed using a Formula (3).

$$y = \delta_{a3} sin \frac{\pi}{l_e} x \tag{3}$$

where l_e is the span length between the HSFRCFST beam's centerline in mm, which is set to 1000 mm in this experiment; δ_{a3} is the vertical displacement at the span's center in mm. The section curvature (φ) of the HSFRCFST beam can be obtained by a second-order derivative.

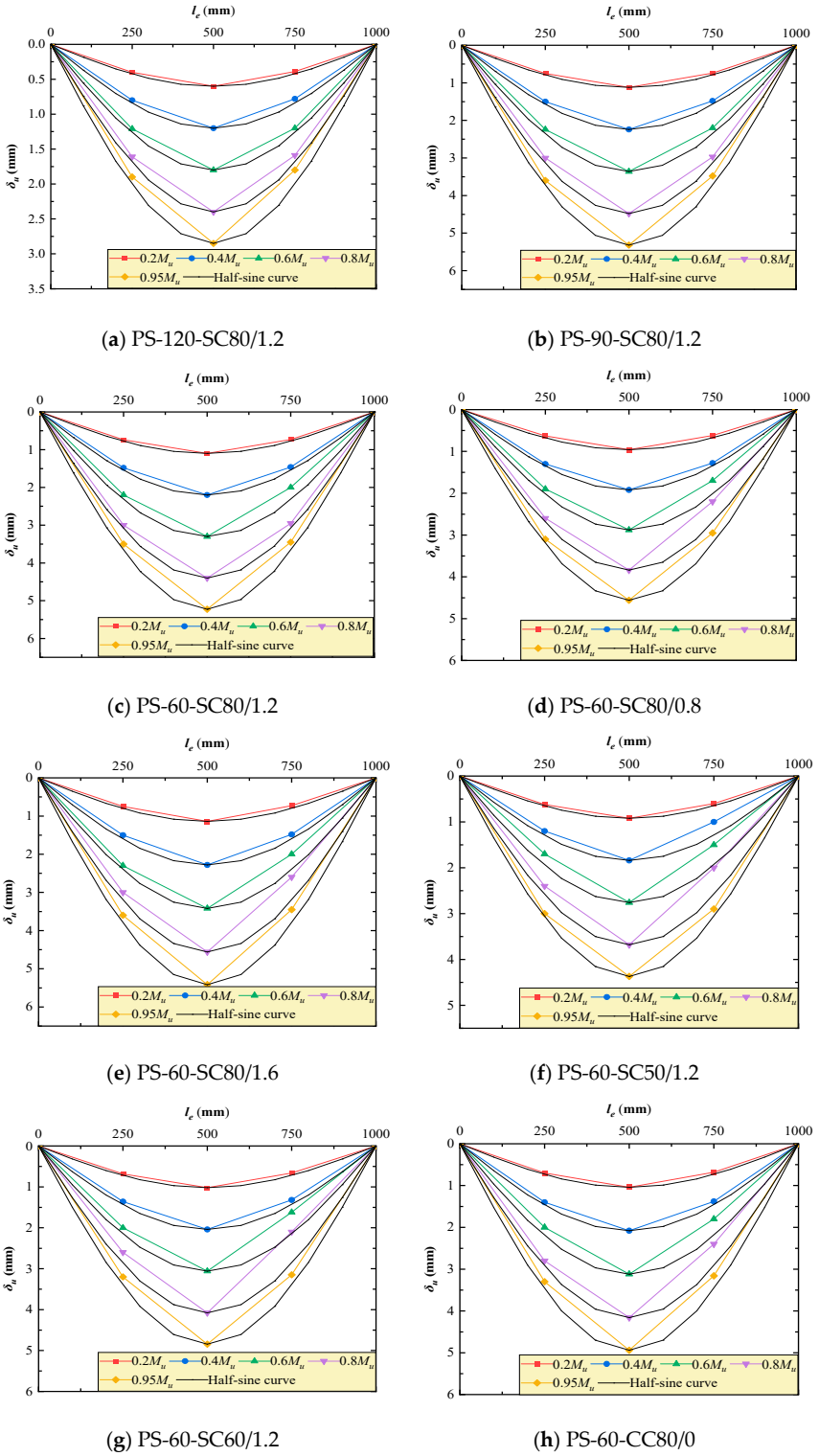

(**a**) PS-120-SC80/1.2 (**b**) PS-90-SC80/1.2

(**c**) PS-60-SC80/1.2 (**d**) PS-60-SC80/0.8

(**e**) PS-60-SC80/1.6 (**f**) PS-60-SC50/1.2

(**g**) PS-60-SC60/1.2 (**h**) PS-60-CC80/0

Figure 7. *Cont.*

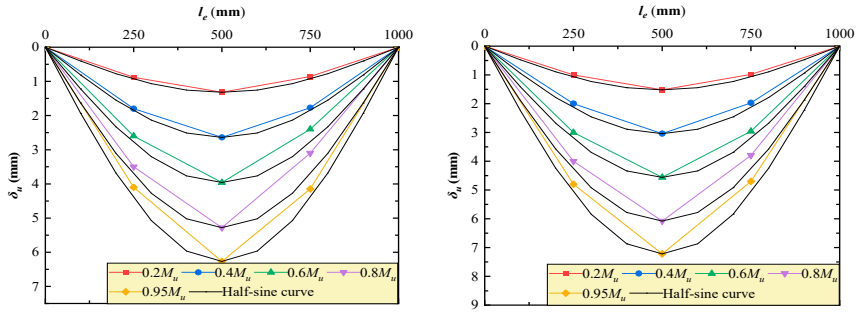

(**i**) SS-0-SC80/1.2 (**j**) NS-0-SC80/1.2

Figure 7. Deflection curves of the experimentally obtained values along the length (unit: mm).

$$\varphi = \delta_{a3}\left(\frac{\pi}{l_e}\right)^2 sin\frac{\pi}{l_e}x \tag{4}$$

In Formula (4), the midspan section curvature (φ_m) can be obtained when x is equal to $l_e/2$.

$$\varphi_m = \delta_{a3}\left(\frac{\pi}{l_e}\right)^2 \tag{5}$$

3.3. Moment–Curvature Behavior

The curves of the midspan moment (M)–curvature (φ_m) of HSFRCFST beams are shown in Figure 8. Formula (6) was used to calculate the midspan moment M values.

$$M = \frac{1}{2}Pa \tag{6}$$

where P represents the applied force measured in kN and a represents the shear span of the HSFRCFST beam (250 mm in this experiment).

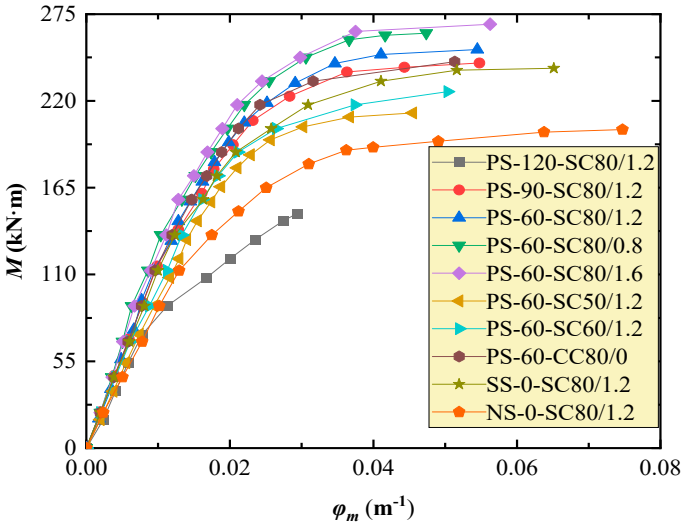

Figure 8. Midspan moment (M)–curvature (φ_m) curves of HSFRCFST beams.

The flexural capacity of HSFRCFST beams was obtained with the exception of the premature failure of PS-60-SC80/1.2 due to end weld cracking. Due to the significant bending stiffness, these curves have a linear climbing portion, a softening part, and no apparent falling segment once the moment capacity is reached. Table 3 lists the bearing properties of HSFRCFST beams.

Table 3. Test results of the beams.

Identifier	δ_u (mm)	B_{si} (kN·m^2)	B_{ss} (kN·m^2)	P_u (kN)	$M_{c,t}$ (kN·m)	$M_{c,c}$ (kN)	$M_{c,t}/M_{c,c}$
PS-120-SC80/1.2	3.0	8588.2	8035.9	1189.8	148.7	--	--
PS-90-SC80/1.2	5.6	11,683.6	10,483.7	1952.2	244.0	252.9	0.965
PS-60-SC80/1.2	5.5	11,445.4	10,921.3	2020.4	252.6	250.2	1.010
PS-60-SC80/0.8	4.8	12,976.9	11,812.2	2103.2	262.9	250.3	1.050
PS-60-SC80/1.6	5.7	12,713.3	12,062.6	2148.8	268.6	260.0	1.033
PS-60-SC50/1.2	4.6	9687.5	9373.0	1698.7	212.3	208.3	1.019
PS-60-SC60/1.2	5.1	11,119.6	10,121.1	1806.8	225.9	231.2	0.977
PS-60-CC80/0	5.2	11,666.6	10,958.9	1959.0	244.9	246.4	0.994
SS-0-SC80/1.2	6.6	11,594.0	10,323.6	1925.5	240.7	252.7	0.953
NS-0-SC80/1.2	7.6	9000.8	8257.6	1614.8	201.9	--	--

3.4. Subsection

Bending stiffness is a crucial criterion for evaluating the local buckling behavior and elastic deformation capacity of CFST beams. In this section, the bending stiffness of HSFRCFST beams is calculated using moment–curvature curves at the midspan. According to Table 3, secant stiffness at 0.2 Mmax is used to establish the initial bending stiffness (B_{si}), while secant stiffness at 0.6 Mmax is used to define the serviceability bending stiffness (B_{ss}). As shown in Table 4, many prediction formulas for the bending stiffness of CFST members have been proposed in existing codes and regulations. Table 5 and Figure 9 show the predicted values for the bending stiffness of the test beam based on current codes and regulations. Prediction values B_1, B_2, B_3, B_4, B_5, and B_6 correspond to the codes GB50936 (2014), DBJ/T13-51-2010 [62], AIJ-SRC (2001) [63], AISC-360 (2016) [64], Euro-code4 (2004) [65], and BS5400 (2005) [66], respectively. B_1/B_{si}, B_2/B_{si}, B_3/B_{si}, B_4/B_{si}, B_5/B_{si}, and B_6/B_{si} have mean values of 1.171, 0.967, 0.612, 0.976, 0.893, and 1.099, respectively, and standard deviations of 0.161, 0.139, 0.099, 0.140, 0.127, and 0.178. B_1/B_{ss}, B_2/B_{ss}, B_3/B_{ss}, B_4/B_{ss}, B_5/B_{ss}, and B_6/B_{ss} have average values of 1.263, 1.043, 0.661, 1.053, 0.963, and 1.187, with standard deviations of 0.170, 0.149, 0.108, 0.150, 0.136, and 0.194, respectively. All existing codes and regulations, with the exception of AIJ-SRC (2001) and Euro-code4 (2004), provide dangerous forecasts for serviceability bending stiffness. The overestimation of the reinforcement effect of infilled concrete by codes and regulations can also be explained. As a result, Euro-code 4 (2004) can predict the bending stiffness of HSFRCFST beams for serviceability.

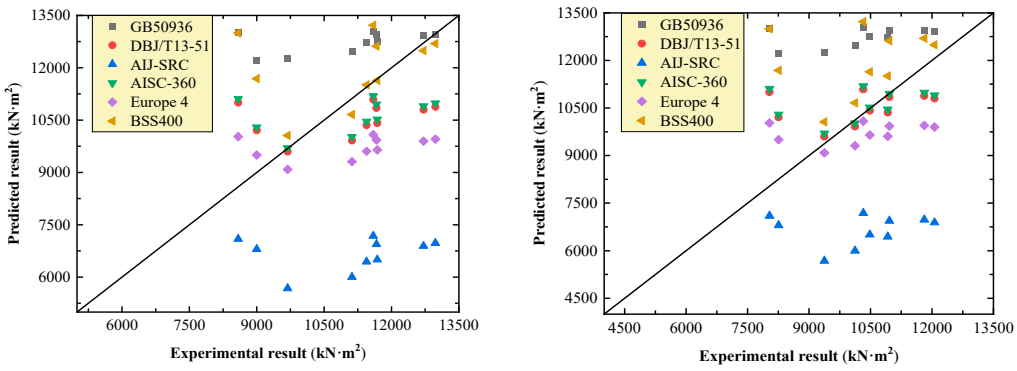

(**a**) Prediction values of B_{si} (**b**) Prediction values of B_{ss}

Figure 9. Prediction values of the bending stiffness (unit: kN·m^2).

Table 4. Prediction formulae for bending stiffness.

Code Number	Recommended Formula	Elastic Modulus Value
GB50936 (2014)	$B_s = E_cI_c + E_sI_s$	E_s = 205,800 MPa; $E_c = 100{,}000/(2.2 + 34.7/f_{cu})$ MPa
DBJ/T13-51-2010	$B_s = E_cI_c + 0.8E_sI_s$	E_s = 206,000 MPa; $E_c = 4700\sqrt{f_c}$ MPa
AIJ-SRC (2001)	$B_s = E_cI_c + 0.2E_sI_s$	E_s = 205,800 MPa; $E_c = 21{,}000\sqrt{f_c/19.6}$ MPa
AISC-360 (2016)	$B_s = E_cI_c + 0.85E_sI_s$	E_s = 210,000 MPa; $E_c = 4700\sqrt{f_c}$ MPa
Europe 4 (2004)	$B_s = E_cI_c + 0.6E_sI_s$	E_s = 206,000 MPa; $E_c = 22{,}000(f_c/10)^{0.3}$ MPa
BS5400 (2005)	$B_s = E_cI_c + E_sI_s$	E_s = 206,000 MPa; $E_c = 450f_{cu}$ MPa

Table 5. Prediction values for bending stiffness of the test beam (unit: kN·m^2).

Identifier	B_1 (kN·m^2)	B_2 (kN·m^2)	B_3 (kN·m^2)	B_4 (kN·m^2)	B_5 (kN·m^2)	B_6 (kN·m^2)
PS-120-SC80/1.2	13,010.0	11,001.1	7095.9	11,103.5	10,028.0	12,994.9
PS-90-SC80/1.2	12,751.1	10,414.7	6504.1	10,517.2	9646.9	11,639.6
PS-60-SC80/1.2	12,720.7	10,354.2	6443.0	10,456.6	9606.5	11,511.6
PS-60-SC80/0.8	12,960.8	10,881.0	6974.7	10,983.4	9951.2	12,693.7
PS-60-SC80/1.6	12,925.2	10,797.6	6890.6	10,900.0	9897.6	12,490.4
PS-60-SC50/1.2	12,258.4	9597.5	5679.4	9700.0	9085.3	10,058.3
PS-60-SC60/1.2	12,481.1	9915.0	5999.8	10,017.5	9308.1	10,660.7
PS-60-CC80/0	12,947.8	10,847.8	6941.2	10,950.2	9929.9	12,618.4
SS-0-SC80/1.2	13,044.4	11,086.8	7182.5	11,189.3	10,082.4	13,220.8
NS-0-SC80/1.2	12,214.1	10,207.6	6802.1	10,297.0	9500.1	11,687.7

As shown in Table 3, the B_{si} values of PS-60-CC80/0, PS-60-SC80/0.8, PS-60-SC80/1.2, and PS-60-SC80/1.6 beams with the same stiffener are 11,666.6 kN·m^2, 12,976.9 kN·m^2, 11,445.4 kN·m^2, and 12,713.3 kN·m^2, respectively. In comparison to the infill conventional concrete with HSFRC, the infill HSFRC with steel fiber volume percentages of 0.8%, 1.2%, and 1.6% increased B_{si} by 11.2%, −1.9%, and 9.0%, respectively, while B_{ss} improved by 7.8%, −0.3%, and 10.1%. These results indicate that steel fiber can enhance bending stiffness to a certain degree. When the steel fiber volume percentage exceeded 0.8%, the enhancement effect became negligible. Adding steel fibers can bridge the matrix of concrete to eliminate internal cracks and transmit stress, thereby sharing the load with uncracked concrete. When the steel fiber content increase, the bonding area between steel fibers and concrete matrix will relatively decrease, and the spacing between steel fibers will also decrease, which will lead to a decrease in bonding strength and weaken the reinforcing effect of steel fibers on concrete, affecting the performance of beams. When the steel fiber content increases to the threshold, the reinforcing effect of steel fibers will be limited due to factors such as dispersion uniformity and bonding strength.

The B_{si} of PS-60-SC50/1.2, PS-60-SC60/1.2, and PS-60-SC80/1.2 HSFRCFST beams with the same steel fiber volume fraction and stiffener type, as seen in Table 3, are 9687.5 kN·m^2, 11,119.6 kN·m^2, and 11,445.4 kN·m^2, respectively. In comparison to PS-60-SC50/1.2 with the desired compressive strength grade of 50 MPa, PS-60-SC60/1.2 with the target compressive strength grade of 60 MPa, and PS-60-SC80/1.2 with the desired compressive strength grade of 80 MPa, B_{si} increased by 14.8% and 18.2%, respectively. These findings demonstrate that the bending stiffness of HSFRCFST beams is significantly impacted by the compressive strength of the infill HSFRC.

According to Table 3, the B_{si} values for PS-120-SC80/1.2, PS-90-SC80/1.2, and PS-60-SC80/1.2 are 8588.2 kN·m^2, 11,683.6 kN·m^2, and 11,445.4 kN·m^2, respectively, based on the equivalent compressive strength and steel fiber volume fraction of the infill HSFRC. In contrast to the B_{si} of PS-120-SC80/1.2, the B_{si} of PS-90-SC80/1.2 and PS-60-SC80/1.2 increased by 36.0% and 33.3%, respectively, while the B_{ss} increased by 30.5% and 35.9%. It is worth noting that PS-60-SC80/1.2 has a higher bending stiffness than its counterparts when the distance between the circular holes is two or three times the diameter. To achieve a higher bending stiffness, the distance between circular holes in HSFRCFST beams with perfobond stiffeners can be two or three times the diameter. In addition, additional circular

concrete dowels reinforce the joint action between the exterior rectangular steel tubes and the infill HSFRC, delaying the buckling of the exterior steel tubes.

As shown in Table 3, the B_{si} values of PS-90-SC80/1.2, SS-0-SC80/1.2, and NS-0-SC80/1.2 HSFRCFST beams with the equivalent compressive strength and steel fiber content of the infill concrete are 11,683.6 kN·m^2, 11,594.0 kN·m^2, and 9000.8 kN·m^2, respectively. In comparison to PS-90-SC80/1.2 with a perfobond stiffener, SS-0-SC80/1.2 with a steel plate stiffener, and NS-0-SC80/1.2 without a stiffener, B_{si} was reduced by 0.8% and 23.0%, respectively, while B_{ss} was reduced by 1.5% and 21.2%. The type of stiffener has a substantial impact on the bending stiffness, and a perfobond stiffener can greatly increase the bending stiffness of HSFRCFST beams.

3.5. Moment Capacity

The value of the moment capacity ($M_{c,t}$) is expressed using Formula (6) and presented in Table 3. Figure 10 displays the relationship between the moment capacity of HSFRCFST beams and the strength grade of infill HSFRC. The moment capacity of HSFRCFST beams rose linearly with infill concrete's compressive strength. When PS-60-SC80/1.2 was compared to PS-60-SC50/1.2, the responding growth rate was 38.1% for infill concrete's compressive strength and 19.0% for moment capacity. According to the experimental findings, the moment capacity is significantly affected by the strength grade of the infill HSFRC.

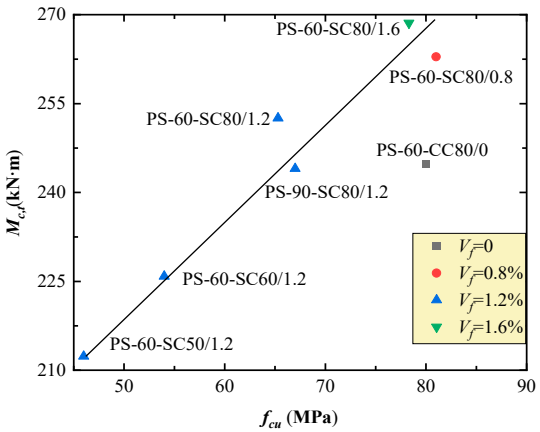

Figure 10. Moment capacity changed with infill concrete strength.

$M_u/f_{sc}\omega_{sc}$ is utilized to remove the impact of infill concrete compressive strength and cross-sectional dimensions on the ultimate load. Figure 11 depicts the response change as the amount of steel fiber rose. The average nominal strength f_{sc} and rectangular section modulus ω_{sc} are determined using Formula (7) and Formula (8), respectively.

$$f_{sc} = f_c(0.07\theta + 1.92) \tag{7}$$

$$\omega_{sc} = \frac{bh^2}{6} \tag{8}$$

where h and b denote the height and width, respectively, of the rectangular section of the HSFRCFST beams.

Using the same strength grade of infill HSFRC, the moment capacity of HSFRCFST beams increases approximately linearly when steel fiber content varies from 0% to 1.6% by volume. It is easier to increase moment capacity when the steel fiber percentage in the research range is 1.2%. This is the amount of steel fiber recommended for use. As the strength grade of the infill HSFRC decreases, the confinement index increases significantly; consequently, the enhancement effect of the moment capacity is improved to some extent.

Based on the analysis of the flexural capacity and the calculation formula proposed by China code GB 50936, the moment capacity of HSFRCFST beams was correlated with the

strength grade of infill HSFRC, the confinement coefficient, rectangular section modulus, and volume percentage of steel fiber, and could be predicted as follows:

$$M_u = \gamma_m \omega_{sc} f_{sc} \tag{9}$$

$$\gamma_m = -5.449 + 3.884 v_f - 8.067\theta + 15.085\sqrt{\theta} \tag{10}$$

where γ_m denotes the plastic development coefficient of the HSFRCFST beams with a rectangular cross-section.

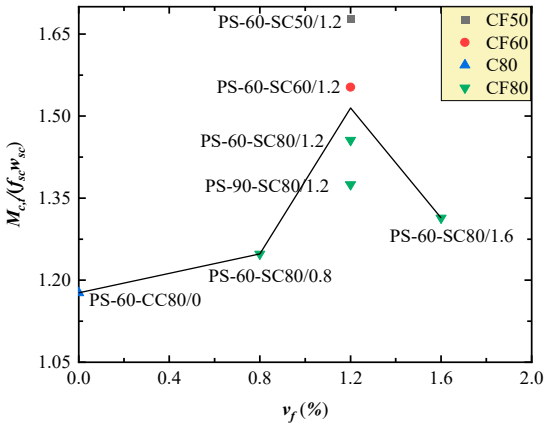

Figure 11. Moment capacity changed with the steel fiber percentage.

Table 3 shows the flexural capacity according to Formula (9). The mean value of M_y/M_c is 1, and the standard deviation is 0.034. This provides support for the idea that the suggested formula may be utilized to reliably determine the flexural capacity of HSFRCFST beams.

3.6. Ductility Index

The CFST beam's deformation performance is commonly quantified using the ductility index (DI), which can be determined using the following Formula (11).

$$DI = \frac{\delta_u - \delta_{hy}}{\delta_{hy}} \tag{11}$$

$$\delta_{hy} = \frac{f_y\left(3l_e^2 - 4a^2\right)}{12E_s h} \tag{12}$$

where δ_u is the maximum vertical displacement of the test beams. The calculated DI is presented in Table 6. Except for the PS-120-SC80/1.2's premature failure, all DI range from 1.16 to 2.57. The results indicate that all of the test beams exhibit excellent ductility.

Table 6. The ductility index and rotational capacity.

Identifier	δ_{hy} (mm)	δ_u (mm)	DI	θ_{limit}	θ_p	R_c
PS-120-SC80/1.2	2.13	3	0.41	0.018850	0.002598	6.26
PS-90-SC80/1.2	2.13	5.6	1.63	0.035186	0.003133	10.23
PS-60-SC80/1.2	2.13	5.5	1.58	0.034558	0.003310	9.44
PS-60-SC80/0.8	2.13	4.8	1.25	0.030159	0.003039	8.92
PS-60-SC80/1.6	2.13	5.7	1.68	0.035814	0.003169	10.30
PS-60-SC50/1.2	2.13	4.6	1.16	0.028903	0.003288	7.79
PS-60-SC60/1.2	2.13	5.1	1.39	0.032044	0.003047	9.52
PS-60-CC80/0	2.13	5.2	1.44	0.032673	0.003148	9.38
SS-0-SC80/1.2	2.13	6.6	2.10	0.041469	0.003114	12.32
NS-0-SC80/1.2	2.13	7.6	2.57	0.047752	0.003364	13.20

3.7. Rotational Capacity

The concrete-filled steel tubular beam must have a rotational capacity (R_c) greater than 3.0, as specified in code AISC-360(2016). According to the analyses in Sections 3.2 and 3.3, there is no softening stage in the moment–curvature curves of the test beams, and the vertical displacement curves can be predicted by the half-sine curve. Consequently, the maximum rotation φ_{max} can be used as the limit rotation φ_{limit}, and the R_c can be expressed by Formula (13).

$$R_c = \frac{\varphi_{limit} - \varphi_p}{\theta_p} \tag{13}$$

$$\varphi_p = \frac{Pa(l_e - a)}{2B_i} \tag{14}$$

$$\varphi_{limit} = \varphi_{max} = \frac{2\delta_u \pi}{l_e} \tag{15}$$

where δ_u is the maximum vertical displacement of the test beams.

Table 6 contains the calculated R_c value. R_c ranges from 6.26 to 13.20, which is greater than 3.0. All of the test beams have sufficient rotational capacity to meet the specifications, as shown by the experimental results.

4. Conclusions

Under pure bending, ten rectangular HSFRCFST beams with stiffeners were investigated experimentally. Based on the experimental data, we can infer the following:

- The bending stiffness and moment capacity of HSFRCFST beams increase when subjected to pure bending by incorporating steel fiber into the infill concrete. When the steel fiber volume percentage is 1.2%, a significant effect can be obtained. The infill HSFRC with steel fiber volume percentages of 0.8%, 1.2%, and 1.6% increases the initial bending stiffness by 11.2%, −1.9%, and 9.0%, respectively. As the steel fiber content increases, the ductility index of the beam also increases. The failure mode of HSFRCFST beams is not drastically changed by the presence of steel fiber. The compressive strength of infill concrete affects the moment capacity and bending stiffness but has a negligible effect on the failure modes.
- The type of stiffener modifies the failure modes of HSFRCFST beams when subjected to pure bending. In comparison to HSFRCFST beams with perfobond stiffener, steel plate stiffener, and without stiffener, the initial bending stiffness is reduced by 0.8% and 23.0%, respectively. The circular hole spacing in perfobond stiffeners may manage the crack spacing of the infill concrete on the tension side, as well as improve the bending stiffness and moment capacity of HSFRCFST beams, and its works optimally with the infill concrete when it is two to three times the diameter.
- The bending stiffness of HSFRCFST beams for serviceability can be predicted using Euro-code 4 (2004). The flexural capacity of HSFRCFST beams can be reliably predicted by the proposed formula. The ductility and rotational capacity of HSFRCFST beams are sufficient for engineering applications.
- Rectangular HSFRCFST beams with stiffeners have good ductility and rotational capacity, which can increase the moment capacity and reduce the member section size. When reinforcing rebars are replaced with ribs, steel tubes, and steel fibers, the engineering expense of HSFRCFST beams is comparable to or somewhat higher than that of ordinary concrete members.

Author Contributions: S.L. (Shiming Liu): Methodology, Investigation, Data Curation, Writing—Original Draft. Z.J.: Formal Analysis, Data Curation. S.L. (Shangyu Li): Conceptualization, Validation. X.L.: Methodology, Investigation. Y.L.: Conceptualization, Methodology, Investigation. S.Z. Conceptualization, Writing—Review and Editing. All authors have read and agreed to the published version of the manuscript.

Funding: This research was funded by the National Natural Science Foundation of China, grant number 51508189; the Fundamental Research Funds for the Central Universities, Chang'an University, grant number 300102211522; the Key Scientific Research Projects in Universities of Henan, China, grant number 23A560006.

Data Availability Statement: Data presented in this research are available upon request from the corresponding author.

Conflicts of Interest: The authors declare no conflicts of interest.

References

1. Deng, Z.; Guo, J.; Yu, J.; Liu, B. Axial Compression Performance of Coral Concrete-Filled Aluminium Tube (CCFAT) Square Stub Columns. *Case Stud. Constr. Mater.* **2021**, *15*, e00697. [CrossRef]
2. Wang, E.; Ding, F.; Wang, L.; Chen, Y.; Sheng, S.; Shen, J.; Lin, Q. Analytical Study on the Composite Behavior of Rectangular CFST Columns under Combined Compression and Torsion. *Case Stud. Constr. Mater.* **2022**, *16*, e01074. [CrossRef]
3. Wei, J.; Xie, Z.; Zhang, W.; Yang, Y.; Luo, X.; Chen, B. Axial Compressive Property of UHPC Plate-CFST Laced Composite Columns. *Case Stud. Constr. Mater.* **2022**, *16*, e01085. [CrossRef]
4. Liu, Y.; Xiong, Z.; Feng, Y.; Jiang, L. Concrete-Filled Rectangular Hollow Section X Joint with Perfobond Leister Rib Structural Performance Study: Ultimate and Fatigue Experimental Investigation. *Steel Compos. Struct.* **2017**, *24*, 455–465.
5. Tian, Z.; Liu, Y.; Jiang, L.; Zhu, W.; Ma, Y. A Review on Application of Composite Truss Bridges Composed of Hollow Structural Section Members. *J. Traffic Transp. Eng. (Engl. Ed.)* **2019**, *6*, 94–108. [CrossRef]
6. Kanishchev, R.; Kvocak, V. Local Buckling of Rectangular Steel Tubes Filled with Concrete. *Steel Compos. Struct.* **2019**, *31*, 201–216.
7. Zeng, J.-J.; Guo, Y.-C.; Liao, J.; Shi, S.-W.; Bai, Y.-L.; Zhang, L. Behavior of Hybrid PET FRP Confined Concrete-Filled High-Strength Steel Tube Columns under Eccentric Compression. *Case Stud. Constr. Mater.* **2022**, *16*, e00967. [CrossRef]
8. Almamoori, A.H.N.; Naser, F.H.; Dhahir, M.K. Effect of Section Shape on the Behaviour of Thin Walled Steel Columns Filled with Light Weight Aggregate Concrete: Experimental Investigation. *Case Stud. Constr. Mater.* **2020**, *13*, e00356. [CrossRef]
9. Cai, J.; Pan, J.; Tan, J.; Vandevyvere, B.; Li, X. Behavior of ECC-Encased CFST Columns under Eccentric Loading. *J. Build. Eng.* **2020**, *30*, 101188. [CrossRef]
10. Cheng, R.; Hu, C.; Gong, M.; Wang, Y. Behaviors of Improved Multi-Cell T-Shaped Concrete-Filled Steel Tubular Columns under Eccentric Loads. *J. Constr. Steel Res.* **2022**, *193*, 107251. [CrossRef]
11. Huang, Y.; Zhao, P.; Lu, Y.; Zhang, H. Push-out Tests of CFST Columns Strengthened with Self-Compacting and Self-Stressing Concrete Filled Square Steel Tube. *J. Constr. Steel Res.* **2022**, *193*, 107263. [CrossRef]
12. Li, G.; Hou, C.; Shen, L. Combined Compression-Bending Performance and Design of CFST with Localised Pitting Corrosion. *J. Constr. Steel Res.* **2022**, *192*, 107247. [CrossRef]
13. Ding, F.; Cao, Z.; Lyu, F.; Huang, S.; Hu, M.; Lin, Q. Practical Design Equations of the Axial Compressive Capacity of Circular CFST Stub Columns Based on Finite Element Model Analysis Incorporating Constitutive Models for High-Strength Materials. *Case Stud. Constr. Mater.* **2022**, *16*, e01115. [CrossRef]
14. Hoang, A.L.; Fehling, E. A Review and Analysis of Circular UHPC Filled Steel Tube Columns under Axial Loading. *Struct. Eng. Mech.* **2017**, *62*, 417–430. [CrossRef]
15. Liu, S.; Ding, X.; Li, X.; Liu, Y.; Zhao, S. Behavior of Rectangular-Sectional Steel Tubular Columns Filled with High-Strength Steel Fiber Reinforced Concrete Under Axial Compression. *Materials* **2019**, *12*, 2716. [CrossRef]
16. Liu, S.; Liu, Y.; Li, X.; Chen, P. Experimental study on steel fiber reinforcement high strength concrete-filled rectangular steel tubular column stiffened with perfobond strip under axial compression. *J. Build. Struct.* **2018**, *39*, 22–28. (In Chinese)
17. Moon, J.; Roeder, C.W.; Lehman, D.E.; Lee, H.-E. Analytical Modeling of Bending of Circular Concrete-Filled Steel Tubes. *Eng. Struct.* **2012**, *42*, 349–361. [CrossRef]
18. Xiong, M.-X.; Xiong, D.-X.; Liew, J.Y.R. Axial Performance of Short Concrete Filled Steel Tubes with High- and Ultra-High-Strength Materials. *Eng. Struct.* **2017**, *136*, 494–510. [CrossRef]
19. Jiang, A.; Chen, J.; Jin, W. Experimental Investigation and Design of Thin-Walled Concrete-Filled Steel Tubes Subject to Bending. *Thin-Walled Struct.* **2013**, *63*, 44–50. [CrossRef]
20. Gu, Z.; Wang, J.; Gao, D.; Zhao, J. Effects of Steel Fibers on the Flexural Behavior of Recycled Concrete Beam: Testing and Analysis. *J. Build. Eng.* **2024**, *85*, 108718. [CrossRef]
21. Hou, C.-C.; Han, L.-H.; Wang, Q.-L.; Hou, C. Flexural Behavior of Circular Concrete Filled Steel Tubes (CFST) under Sustained Load and Chloride Corrosion. *Thin-Walled Struct.* **2016**, *107*, 182–196. [CrossRef]
22. Montuori, R.; Piluso, V. Analysis and Modelling of CFT Members: Moment Curvature Analysis. *Thin-Walled Struct.* **2015**, *86*, 157–166. [CrossRef]
23. İpek, S.; Erdoğan, A.; Güneyisi, E.M. Compressive Behavior of Concrete-Filled Double Skin Steel Tubular Short Columns with the Elliptical Hollow Section. *J. Build. Eng.* **2021**, *38*, 102200. [CrossRef]
24. Qiu, W.; McCann, F.; Espinos, A.; Romero, M.L.; Gardner, L. Numerical Analysis and Design of Slender Concrete-Filled Elliptical Hollow Section Columns and Beam-Columns. *Eng. Struct.* **2017**, *131*, 90–100. [CrossRef]

25. Liu, Z.; Lu, Y.; Li, S.; Zong, S.; Yi, S. Flexural Behavior of Steel Fiber Reinforced Self-Stressing Recycled Aggregate Concrete-Filled Steel Tube. *J. Clean. Prod.* **2020**, *274*, 122724. [CrossRef]
26. Wang, R.; Han, L.-H.; Nie, J.-G.; Zhao, X.-L. Flexural Performance of Rectangular CFST Members. *Thin-Walled Struct.* **2014**, *79*, 154–165. [CrossRef]
27. Chung, K.S.; Kim, J.H.; Yoo, J.H. Experimental and Analytical Investigation of High-Strength Concrete-Filled Steel Tube Square Columns Subjected to Flexural Loading. *Steel Compos. Struct.* **2013**, *14*, 133–153. [CrossRef]
28. Hou, W.-Q.; Yang, J.-J.; Zhang, Z.-X.; Yuan, X.-Q. Experimental Study and Application of Manufactured Sand Self-Compacting Concrete in Concrete-Filled-Steel-Tube Arch Bridge: A Case Study. *Case Stud. Constr. Mater.* **2021**, *15*, e00718. [CrossRef]
29. Javed, M.F.; Sulong, N.H.R.; Memon, S.A.; Rehman, S.K.U.; Khan, N.B. FE Modelling of the Flexural Behaviour of Square and Rectangular Steel Tubes Filled with Normal and High Strength Concrete. *Thin-Walled Struct.* **2017**, *119*, 470–481. [CrossRef]
30. Younas, S.; Li, D.; Hamed, E.; Uy, B. Behaviour of High Strength Concrete-Filled Short Steel Tubes under Sustained Loading. *Steel Compos. Struct.* **2021**, *39*, 159–170.
31. Ding, F.; Luo, L.; Zhu, J.; Wang, L.; Yu, Z. Mechanical Behavior of Stirrup-Confined Rectangular CFT Stub Columns under Axial Compression. *Thin-Walled Struct.* **2018**, *124*, 136–150. [CrossRef]
32. Lian, W.; Dong, J.; Wang, Q. Axial Compressive Behavior of Concrete-Filled Steel Tube Columns with Stiffeners. *Steel Compos. Struct.* **2018**, *29*, 151–159.
33. Peng, K.; Yu, T.; Hadi, M.N.S.; Huang, L. Compressive Behavior of Hybrid Double-Skin Tubular Columns with a Rib-Stiffened Steel Inner Tube. *Compos. Struct.* **2018**, *204*, 634–644. [CrossRef]
34. Thomas, J.; Sandeep, T.N. Experimental Study on Circular CFST Short Columns with Intermittently Welded Stiffeners. *Steel Compos. Struct.* **2018**, *29*, 659–667.
35. Wang, Z.-B.; Tao, Z.; Yu, Q. Axial Compressive Behaviour of Concrete-Filled Double-Tube Stub Columns with Stiffeners. *Thin-Walled Struct.* **2017**, *120*, 91–104. [CrossRef]
36. Du, Y.; Chen, Z.; Wang, Y.-B.; Richard Liew, J.Y. Ultimate Resistance Behavior of Rectangular Concrete-Filled Tubular Beam-Columns Made of High-Strength Steel. *J. Constr. Steel Res.* **2017**, *133*, 418–433. [CrossRef]
37. Li, G.; Liu, D.; Yang, Z.; Zhang, C. Flexural Behavior of High Strength Concrete Filled High Strength Square Steel Tube. *J. Constr. Steel Res.* **2017**, *128*, 732–744. [CrossRef]
38. Ramkumar, K.B.; Rajkumar, P.R.K.; Gunasekaran, K. Performance of Hybrid Steel Fiber-Reinforced Self-Compacting Concrete RC Beam under Flexure. *Eng. Sci. Technol.* **2023**, *42*, 101432.
39. Silva, A.; Jiang, Y.; Castro, J.M.; Silvestre, N.; Monteiro, R. Experimental Assessment of the Flexural Behaviour of Circular Rubberized Concrete-Filled Steel Tubes. *J. Constr. Steel Res.* **2016**, *122*, 557–570. [CrossRef]
40. Silva, A.; Jiang, Y.; Castro, J.M.; Silvestre, N.; Monteiro, R. Monotonic and Cyclic Flexural Behaviour of Square/Rectangular Rubberized Concrete-Filled Steel Tubes. *J. Constr. Steel Res.* **2017**, *139*, 385–396. [CrossRef]
41. Silva, A.; Jiang, Y.; Macedo, L.; Castro, J.M.; Monteiro, R.; Silvestre, N. Seismic Performance of Composite Moment-Resisting Frames Achieved with Sustainable CFST Members. *Front. Struct. Civ. Eng.* **2016**, *10*, 312–332. [CrossRef]
42. Xiong, M.-X.; Xiong, D.-X.; Liew, J.Y.R. Flexural Performance of Concrete Filled Tubes with High Tensile Steel and Ultra-High Strength Concrete. *J. Constr. Steel Res.* **2017**, *132*, 191–202. [CrossRef]
43. Dong, M.; Elchalakani, M.; Karrech, A.; Hassanein, M.F.; Xie, T.; Yang, B. Behaviour and Design of Rubberised Concrete Filled Steel Tubes under Combined Loading Conditions. *Thin-Walled Struct.* **2019**, *139*, 24–38. [CrossRef]
44. Duarte, A.P.C.; Silva, B.A.; Silvestre, N.; De Brito, J.; Júlio, E.; Castro, J.M. Finite Element Modelling of Short Steel Tubes Filled with Rubberized Concrete. *Compos. Struct.* **2016**, *150*, 28–40. [CrossRef]
45. Ding, X.; Li, C.; Han, B.; Lu, Y.; Zhao, S. Effects of Different Deformed Steel-Fibers on Preparation and Fundamental Properties of Self-Compacting SFRC. *Constr. Build. Mater.* **2018**, *168*, 471–481. [CrossRef]
46. Mou, T.M.; Zhou, X.J.; Fan, B.K.; Ding, Q.J. Frost Resistance of Steel Fiber Reinforced Micro-Expansive Concrete Filled Steel Tube. *Appl. Mech. Mater.* **2012**, *204–208*, 3956–3960. [CrossRef]
47. Chen, J.; Liu, X.; Liu, H.; Zeng, L. Axial Compression Behavior of Circular Recycled Concrete-Filled Steel Tubular Short Columns Reinforced by Silica Fume and Steel Fiber. *Steel Compos. Struct.* **2018**, *27*, 193–200.
48. Lu, Y.; Li, N.; Li, S.; Liang, H. Behavior of Steel Fiber Reinforced Concrete-Filled Steel Tube Columns under Axial Compression. *Constr. Build. Mater.* **2015**, *95*, 74–85. [CrossRef]
49. Lu, Y.; Liu, Z.; Li, S.; Hu, J. Axial Compression Behavior of Hybrid Fiber Reinforced Concrete Filled Steel Tube Stub Column. *Constr. Build. Mater.* **2018**, *174*, 96–107. [CrossRef]
50. Guler, S.; Yavuz, D. Post-Cracking Behavior of Hybrid Fiber-Reinforced Concrete-Filled Steel Tube Beams. *Constr. Build. Mater.* **2019**, *205*, 285–305. [CrossRef]
51. Li, C.; Geng, H.; Deng, C.; Li, B.; Zhao, S. Experimental Investigation on Columns of Steel Fiber Reinforced Concrete with Recycled Aggregates under Large Eccentric Compression Load. *Materials* **2019**, *12*, 445. [CrossRef] [PubMed]
52. Choi, C.S.; Jung, H.S.; Choi, H.K. Behaviour of Concrete Filled Steel Square-Tube Stub Column with Steel-Fiber Reinforced High Strength Concrete. *Adv. Mater. Res.* **2013**, *663*, 125–129. [CrossRef]
53. Ding, X.; Li, C.; Li, Y.; Lu, Y.; Song, C.; Zhao, S. Experimental and Numerical Study on Stress-Strain Behavior of Self-Compacting SFRC under Uniaxial Compression. *Constr. Build. Mater.* **2018**, *185*, 30–38. [CrossRef]

54. Hou, Z.; Nordin, N. Flexural Behavior of Inverted Steel Fiber-Reinforced Concrete T-Beams Reinforced with High-Yield Steel Bars. *Buildings* **2024**, *14*, 891. [CrossRef]
55. *GB/T 50081-2019*; Standard for Test Methods of Concrete Physical and Mechanical Properties. China Building Industry Press: Beijing, China, 2019.
56. *JG/T 472-2015*; Steel Fiber Reinforced Concrete. Standards Press of China: Beijing, China, 2015.
57. *GB 50666-2011*; Code for Construction of Concrete Structures. China Building Industry Press: Beijing, China, 2011.
58. *GB 50661-2011*; Code for Welding of Steel Structures. China Building Industry Press: Beijing, China, 2011.
59. *DG/TJ08-2089-2012*; Technical Specification for Lightweight Steel Building Structures. Tong Ji University Press: Shanghai, China, 2012.
60. *GB/T 228.1-2021*; Metallic Materials—Tensile Testing—Part 1: Method of Test at Room Temperature. Standards Press of China: Beijing, China, 2021.
61. *GB 50936-2014*; Technical Code for Concrete Filled Steel Tubular Structures. China Building Industry Press: Beijing, China, 2014.
62. *DBJ/T13-51-2010*; Technical Specification for Concrete-Filled Steel Tubular Structures. Fujian Province Department of Housing and Urban-Rural Development: Fujian, China, 2010.
63. *AIJ-SRC (2001)*; The Standard for Structure Calculation of Steel Reinforced Concrete Structures. Architectural Institute of Japan: Tokyo, Japan, 2001.
64. *ANSI/AISC 360-16*; Specification for Structural Steel Buildings. American Institute of Steel Construction: Detroit, MI, USA, 2016.
65. *Euro Code 4 (2004)*; Design of Composite Steel and Concrete Structures. British Standards Institution: London, UK, 2004.
66. *BS5400(2005)*; Steel, Concrete and Composite Bridges Part 4: Code of Practice for Design of Concrete Bridges. British Standard Institution: London, UK, 2005.